CELL BIOLOGY

Nutrient availability shapes methionine metabolism in p16/*MTAP*-deleted cells

Sydney M. Sanderson, Peter G. Mikhael, Vijyendra Ramesh, Ziwei Dai, Jason W. Locasale*

Codeletions of gene loci containing tumor suppressors and neighboring metabolic enzymes present an attractive synthetic dependency in cancers. However, the impact that these genetic events have on metabolic processes, which are also dependent on nutrient availability and other environmental factors, is unknown. As a proof of concept, we considered panels of cancer cells with homozygous codeletions in *CDKN2a* and *MTAP*, genes respectively encoding the commonly-deleted tumor suppressor p16 and an enzyme involved in methionine metabolism. A comparative metabolomics analysis revealed that while a metabolic signature of *MTAP* deletion is apparent, it is not preserved upon restriction of nutrients related to methionine metabolism. Furthermore, re-expression of *MTAP* exerts heterogeneous consequences on metabolism across isogenic cell pairs. Together, this study demonstrates that numerous factors, particularly nutrition, can overwhelm the effects of metabolic gene deletions on metabolism. These findings may also have relevance to drug development efforts aiming to target methionine metabolism.

INTRODUCTION

Metabolic phenotypes arise from a complex interaction between genes and the environment. Determinants of these phenotypes include the genomic encoding of metabolic genes and their sequence variants, transcriptional and allosteric regulation of metabolic enzyme activity, and nutrient availability. Despite this complexity, the prospect of targeting metabolism for therapy is attractive because of both the relative drugability of metabolic enzymes and the numerous metabolic alterations observed in pathological conditions such as in cancer. Nevertheless, principled strategies that define context-specific metabolic differences are desired.

One example of identifying these contexts considers the observation that genetic deletions of tumor suppressor genes are often accompanied by codeletion of neighboring genes, many of which encode metabolic enzymes. For example, approximately 15% of cancers exhibit homozygous deletions of the *CDKN2a* locus, which encodes for the tumor suppressor p16, with 80 to 90% of these tumors also exhibiting concurrent deletion of a proximal gene, *MTAP*, that encodes for the methionine salvage enzyme methylthioadenosine phosphorylase (MTAP) (*1*, *2*). A number of studies have investigated *MTAP* deletion as a possible collateral lethality and have identified vulnerabilities in this subset of cancers (*3*–*7*) with several investigating some of the effects of *MTAP* deletion on methionine metabolism (*8*–*10*). However, a systematic comparison of the relative effects of *MTAP* deletion as it relates to other variables that have been shown to shape metabolism is lacking.

The recycling of the essential amino acid methionine (i.e., methionine salvage) is an integral component of a metabolic network known as one-carbon metabolism (*11*–*14*). This network integrates nutrients, such as glucose and dietary amino acids (including serine, cysteine, and methionine), for use in various biological processes such as phospholipid synthesis, redox maintenance, and production of substrates for methylation reactions (*15*–*19*). Changes to the availability of these nutrients have been shown to exert major effects on the metabolism of this pathway; for example, methionine concentrations in human plasma were shown to positively correlate with levels of methylated metabolites (*15*), and dietary serine has been found to directly affect tumor growth (*20*, *21*). Moreover, it has been demonstrated in many contexts that the same tumorigenic genetic alteration can have markedly different metabolic consequences depending on the tissue of origin (*22*, *23*).

Using a metabolomics approach (*24*–*27*), this current study quantifies the impact of *MTAP* deletion on metabolism in the context of cell type and the availability of nutrients related to methionine metabolism. We find that while *MTAP* deletion produces a defined metabolic signature, this signature is diminished upon consideration of the changes to metabolism that result from the availability of nutrients related to methionine and one-carbon metabolism. Furthermore, these changes vary widely across individual cell lines and are not predicted by *MTAP* status. Thus, upon consideration of other variables that shape metabolic processes, *MTAP* status alone appears to exert a relatively modest effect on cellular metabolism.

RESULTS

MTAP status has a defined metabolic signature

MTAP uses the substrate methylthioadenosine (MTA) to allow for the recycling of methionine back into the methionine cycle (Fig. 1A). To investigate the impact of its deletion on metabolism, we first assembled a panel of 10 genetically diverse tissue-matched cancer cell lines, with each pair composed of one cell line characterized by homozygous deletions of *CDKN2a* and *MTAP* ($MTAP^{-/-}$) and the other exhibiting no alterations in this chromosomal locus ($MTAP^{+/+}$); the presence or absence of *MTAP* protein was verified by immunoblotting (Fig. 1B), and Cdkn2a mRNA expression was assessed using RNA sequencing data for these cell lines (fig. S1A). Using liquid chromatography coupled with high-resolution mass spectrometry (LC-HRMS), we analyzed the levels of more than 200 metabolites between the cell lines in standard culture conditions to assess global metabolic profiles of each line (fig. S1B). Extending on previous studies that found that *MTAP* status could predict differential MTA levels (*8*–*10*), we found that MTA was the most differentially abundant

Department of Pharmacology and Cancer Biology, Duke University School of Medicine, Durham, NC 27710, USA.
*Corresponding author. Email: jason.locasale@duke.edu

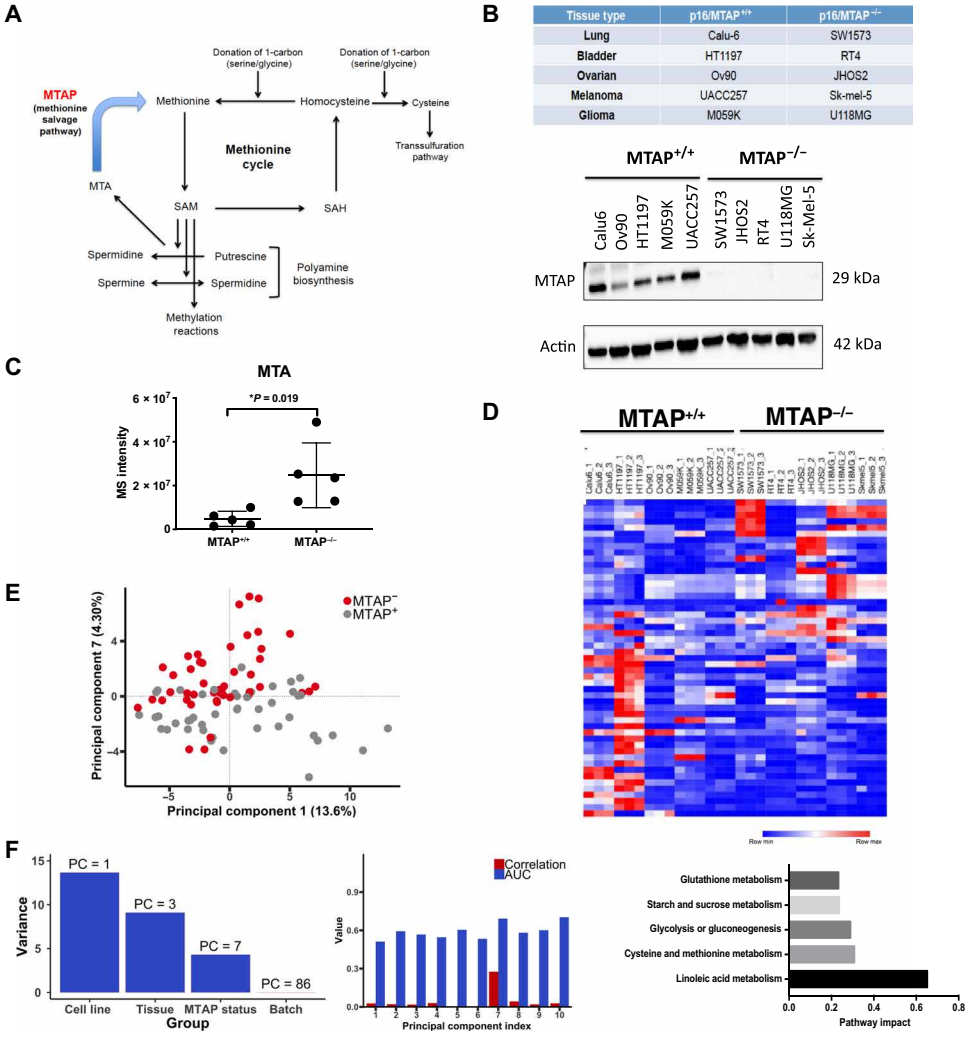

Fig. 1. Cancer cell lines exhibiting homozygous deletion of *MTAP* show altered patterns of metabolite levels. (**A**) Methionine cycle. Methionine can be recycled from homocysteine via a donation from serine or glycine or salvaged by *MTAP* via conversion of the polyamine biosynthesis by-product MTA. SAM, s-adenosyl-methionine; SAH, s-adenosyl-homocysteine. (**B**) Cancer cell line panel of 10 lines from five different tissues, exhibiting either wild-type or homozygous deletion of p16/*MTAP*. Western blot validation of *MTAP* deletion. (**C**) Integrated intensity values (relative metabolite abundance) of MTA in $MTAP^{+/+}$ versus $MTAP^{-/-}$ cell lines. *P* values were obtained from Student's *t* test. (**D**) Heat map of top 50 differential metabolites between $MTAP^{+/+}$ and $MTAP^{-/-}$ cell lines. Top affected pathways are indicated. (**E**) PCA of variance between $MTAP^{+/+}$ and $MTAP^{-/-}$ groups. (**F**) Assignment of principal component (PC) that displays greatest variance between the indicated groups. AUC, area under the curve.

metabolite between the two groups, with *MTAP*-deleted lines exhibiting significantly higher levels of MTA compared to *MTAP*-expressing lines (Fig. 1C).

We next identified the top 50 differential metabolites between the $MTAP^{+/+}$ and $MTAP^{-/-}$ lines. When these metabolites were visualized using unsupervised hierarchical clustering, a pattern (i.e., *MTAP* "signature") was evident (Fig. 1D and table S1). Network-based pathway analysis (Methods) of these metabolites indicated that the metabolic profiles of $MTAP^{-/-}$ lines differed from those of $MTAP^{+/+}$ lines predominantly via differential activity of cysteine metabolism and glycolysis, consistent with our initial observations (Fig. 1D).

We then performed principal components analysis (PCA) to determine the extent to which *MTAP* status segregated the metabolic profiles of the cell lines (Fig. 1E). We found that the seventh principal component (PC7) best separated the two groups, accounting for 4.3% of the overall variance (Fig. 1F). Comparatively, PC3 (accounting for ~8% of the variance) best separated the cell lines by tissue type. Of note, most of the variance was linked to the individual cell line (i.e., each cell line distinctly clustered from each other). These findings indicate that while *MTAP* deletion does induce a reproducible metabolic shift, heterogeneity between cell lines is a larger source of variation compared to tissue type, which accounted for almost twice as much variation as *MTAP* status (Fig. 1F).

Responsiveness to methionine availability is not predicted by *MTAP* status

In basal conditions, an *MTAP*-associated metabolic signature is readily apparent; however, metabolism has been shown to be heavily influenced by nutrient availability and other environmental factors (*15*, *22*, *28*). Therefore, we next sought to determine whether *MTAP*-deleted lines would exhibit enhanced responsiveness to nutrient availability, particularly methionine restriction. We hypothesized that under these conditions, *MTAP*-associated metabolism would

be affected because of an inability to salvage methionine from MTA. To test this, we cultured each cell line in either complete (100 μM methionine, or Met^+) or methionine-restricted (3 μM methionine, or Met^-) medium for 24 hours and used LC-HRMS to define the metabolic consequences of methionine restriction across the cell lines (Fig. 2A). Previous work has shown that 3 μM is the lower limit of what is observed in human plasma (*15*), whereas 100 μM is the value in typical cell culture conditions.

Following unsupervised hierarchical clustering of both the individual samples and the fold changes of metabolites, pathway analysis demonstrated that particular metabolic pathways tended to cluster together (such as fatty acid metabolism with tryptophan and phenylalanine metabolism) as well as pathways involved in one-carbon metabolism (including serine, glycine, cysteine, and methionine metabolism); however, cell lines did not cluster by *MTAP* status or tissue type, demonstrating that metabolic responsiveness to methionine restriction is not defined or predicted by these factors in cell culture (Fig. 2B).

MTA levels were significantly diminished in all except 1 (Sk-Mel-5) of 10 cell lines upon methionine restriction (Fig. 2C). When we analyzed the number of significantly altered metabolites that were methionine related (i.e., within five biochemical reactions) or methionine unrelated (greater than five reactions away), $MTAP^{-/-}$ lines were not found to exhibit a greater degree of altered methionine metabolism compared to $MTAP^{+/+}$ lines upon methionine restriction (Fig. 2D). Furthermore, PCA conducted for fold change values of each metabolite demonstrated that although cell lines tended to cluster by *MTAP* status to a greater extent than by tissue of origin, most of the variance was accounted for by cell line–to–cell line variability (fig. S2B), and cell lines that exhibited higher responsiveness to methionine restriction were not classified by similar *MTAP* status or tissue type (fig. S2C).

Of particular interest was the finding that when fold change values of each metabolite were averaged across the five cell lines within each group, methionine restriction appeared to have little to no effect on global metabolism (Fig. 2E and fig. S2D); in contrast, methionine restriction appeared to have a substantial yet highly variable effect when fold changes were analyzed in each cell line (fig. S2E). To further illustrate this finding, we examined alterations in key metabolites of the transsulfuration pathway, which is downstream of the methionine cycle and provides glutathione for intracellular redox reactions (Fig. 2F). Independent of *MTAP* status, some cell lines demonstrated significant alterations throughout this pathway, while others appeared to show no changes as a result of methionine restriction. Furthermore, the alterations that were induced were unexpectedly variable between cell lines; for instance, glutathione was found to increase twofold in the $MTAP^{+/+}$ melanoma line UACC-257 upon methionine restriction, while it decreased by almost half in the $MTAP^{-/-}$ bladder line RT4 and was nonsignificantly altered in most of the other cell lines (Fig. 2F). Together, these findings illustrate that the responsiveness to alterations in methionine availability is not predicted by *MTAP* status and is notably heterogeneous between cell lines, and that accumulation of MTA, which is the key feature of the *MTAP* metabolic signature, can be abrogated by methionine restriction.

Responsiveness to alterations in other one-carbon nutrient availability is largely *MTAP* status independent

Although *MTAP* status did not appear to be predictive of responsiveness to methionine availability, we further hypothesized that the *MTAP*-deleted lines may have adapted to the inability to salvage methionine by differentially regulating the utilization of nutrients that feed into and out of the methionine cycle. To test this, we cultured the cell lines either in serine-restricted (~16 μM from 10% serum compared to ~280 μM) medium for 24 hours or in cysteine-restricted (~6 μM from 10% serum compared to ~200 μM) medium for 6 hours and validated the reduction in levels of the respective amino acid (Fig. 3A and fig. S3A). Of note, a shorter culture time for the cysteine restriction experiments was used because of the highly variable toxicity of the 24-hour cysteine restriction across the panel of cell lines independent of *MTAP* status (fig. S3B). As observed with methionine restriction, cell lines did not appear to globally respond to either serine or cysteine restriction in an *MTAP* status–dependent manner, and the new metabolic state that arose from altered nutrient availability was independent of *MTAP* status (Fig. 3B).

Serine restriction appeared to induce an increase in MTA levels in three of five $MTAP^{+/+}$ lines and in one $MTAP^{-/-}$ line while producing no significant change in MTA levels in the other lines; conversely, cysteine restriction mostly induced a decrease in MTA levels in both groups (Fig. 3C). Similar to what was found with methionine restriction, when the fold changes of metabolites were averaged across the five cell lines for each group, serine restriction was found to have no significantly reproducible and general impact on global metabolism (Fig. 3D and fig. S3C) although each cell line demonstrated responsiveness to the restriction when examined individually (Fig. 3E). In contrast, averaging fold changes across the respective cell lines showed that both groups responded similarly to cysteine restriction, as evidenced by significant reductions in cysteine-related metabolites such as cysteate and oxidized glutathione (Fig. 3D and fig. S3C); however, each cell line still exhibited a unique metabolic response to the restriction as was found in the other nutrient restriction conditions (Fig. 3E). Furthermore, the tissue of origin was found to account for more variance in the data than the *MTAP* status, although both were again found to account for substantially less of the variance compared to heterogeneity between cell lines (fig. S3, D and E).

Cysteate (an intermediate in taurine biosynthesis) levels were found to be consistently depleted across all cell lines in response to cysteine restriction; however, closer examination of this pathway demonstrated that with the exception of one cell line (SW1573), taurine and hypotaurine levels tended to be altered less in $MTAP^{-/-}$ cell lines compared to $MTAP^{+/+}$ cell lines (Fig. 3F). These findings could imply that $MTAP^{-/-}$ cells adapt to deficiencies in recycling methionine by becoming less dependent on cysteine availability, although *MTAP*-deleted lines, on average, did not show decreased cytotoxicity in cysteine-restricted conditions compared to *MTAP*-positive lines (fig. S3A). Together, these results show that, in terms of the factors mediating responsiveness to one-carbon nutrient availability, the resulting metabolic state is largely *MTAP* status independent and is better predicted by other contextual factors.

Restoration of *MTAP* expression produces heterogeneous effects on metabolism

We next sought to determine whether reexpression of *MTAP* protein in *MTAP*-deleted cell lines would induce similar metabolic effects both on responsiveness to nutrient restriction and on overall metabolism. We ectopically expressed *MTAP* or a green fluorescent protein (GFP) control in four *MTAP*-deleted cell lines (Fig. 4A) and demonstrated that the resulting protein was functional as evidenced by a reduction in MTA levels in *MTAP*-expressing cells compared

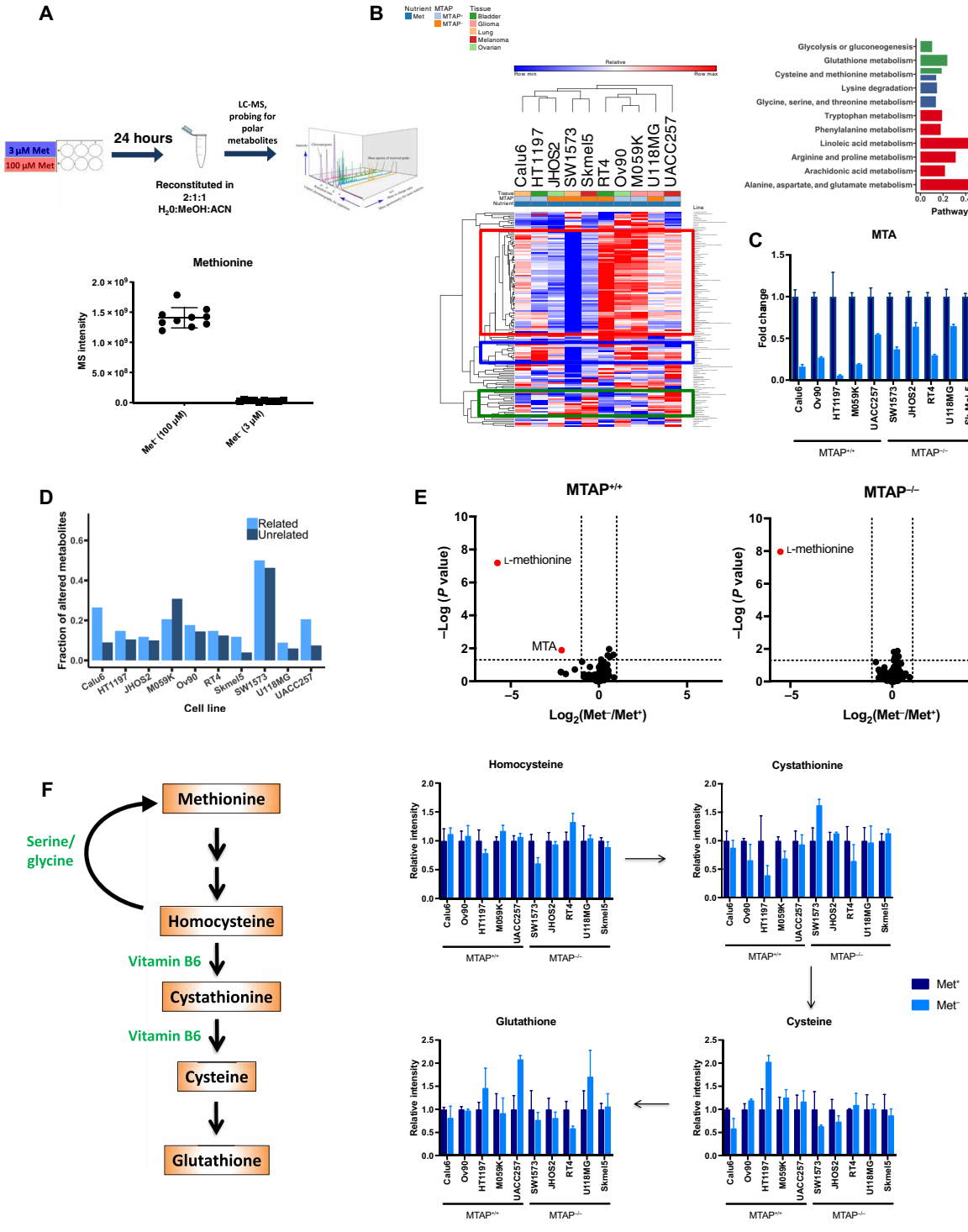

Fig. 2. Responsiveness to methionine availability is heterogeneous and is not predicted by *MTAP* status. (**A**) Experimental setup and validation of methionine restriction. Each dot corresponds to the integrated intensity of detected methionine (averaged across three replicates) in each cell line for the indicated culture conditions. LC-MS, liquid chromatography–mass spectrometry. (**B**) Heat map of fold changes in global metabolite levels upon methionine restriction, hierarchically clustered by cell lines and metabolites. Top affected pathways are indicated. (**C**) Fold change values of MTA metabolite levels either in complete (100 μM Met, or Met^+) or restricted (~3 μM Met, or Met^-). (**D**) Fraction of significantly altered ($P < 0.05$) metabolites that are related (i.e., within five reactions) or unrelated to methionine. (**E**) Volcano plot of fold change (Met^-/Met^+) values of metabolites, averaged across either $MTAP^{+/+}$ or $MTAP^{-/-}$ groups. *P* values obtained using Student's *t* test. (**F**) Example of heterogeneous responsiveness to methionine restriction, as indicated by fold change in metabolites involved in the transsulfuration pathway.

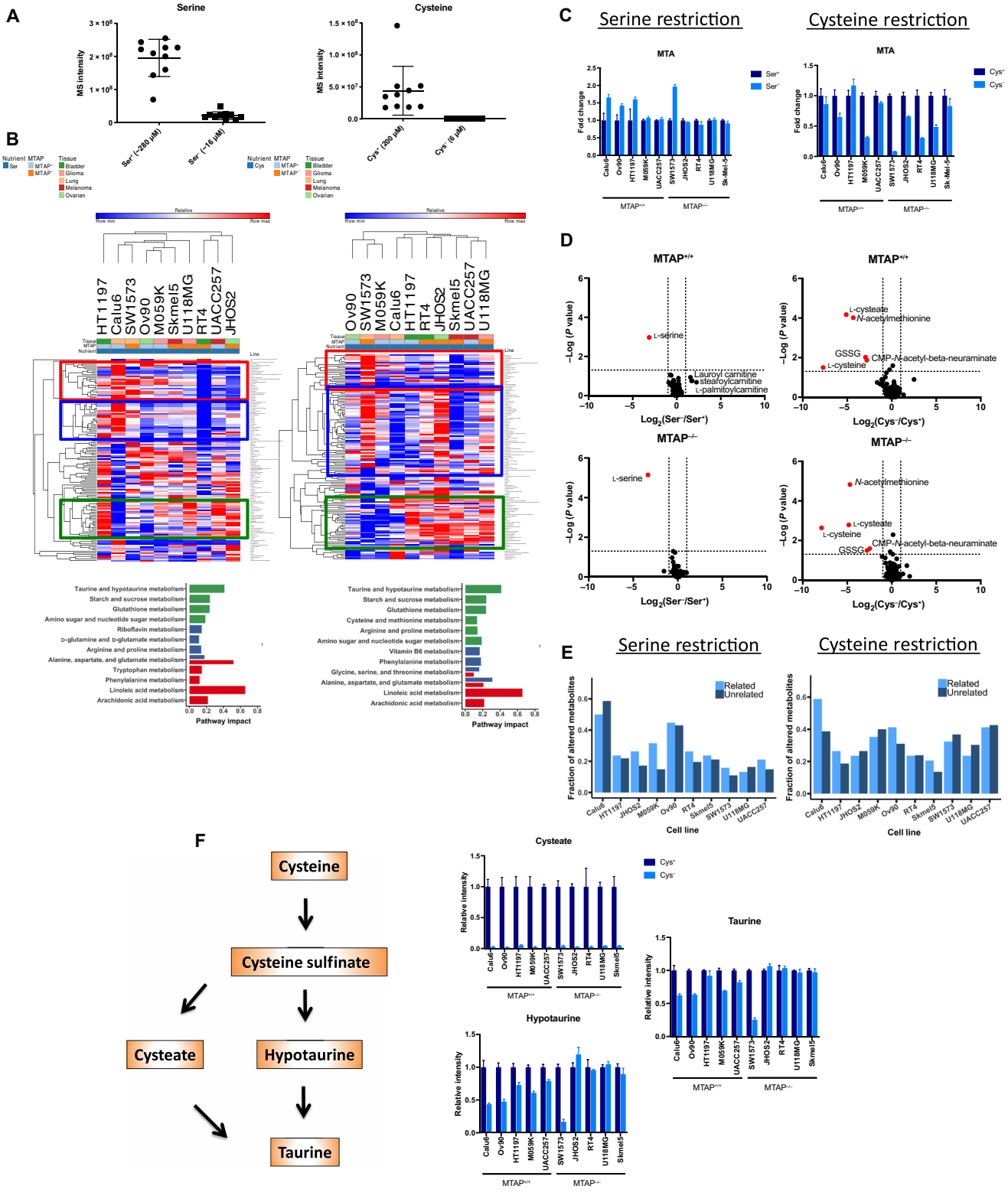

Fig. 3. Responsiveness to alterations in other one-carbon nutrient availability is largely *MTAP* status independent. (**A**) Validation of serine and cysteine restriction. (**B**) Heat map of fold changes in global metabolite levels upon serine (left) and cysteine (right) restriction, hierarchically clustered by cell lines and metabolites. Top affected pathways are indicated. (**C**) Fold change values of MTA metabolite levels either in complete (280 μM Ser, or Ser^+, and 200 μM Cys, or Cys^+) or restricted (~16 μM Ser, or Ser^-, and 6 μM Cys, or Cys^-) medium. (**D**) Volcano plot of fold change (Ser^-/Ser^+ or Cys^-/Cys^+) values of metabolites, averaged across either $MTAP^{+/+}$ or $MTAP^{-/-}$ groups. *P* values obtained using Student's *t* test. GSSG, oxidized glutathione; CMP, cytidine 5′-monophosphate. (**E**) Fraction of significantly altered ($P < 0.05$, Student's *t* test) metabolites that are related (i.e., within five reactions) or unrelated to serine (left) and cysteine (right). (**F**) Alterations in relative metabolite levels upon cysteine restriction in metabolites involved in taurine biosynthesis.

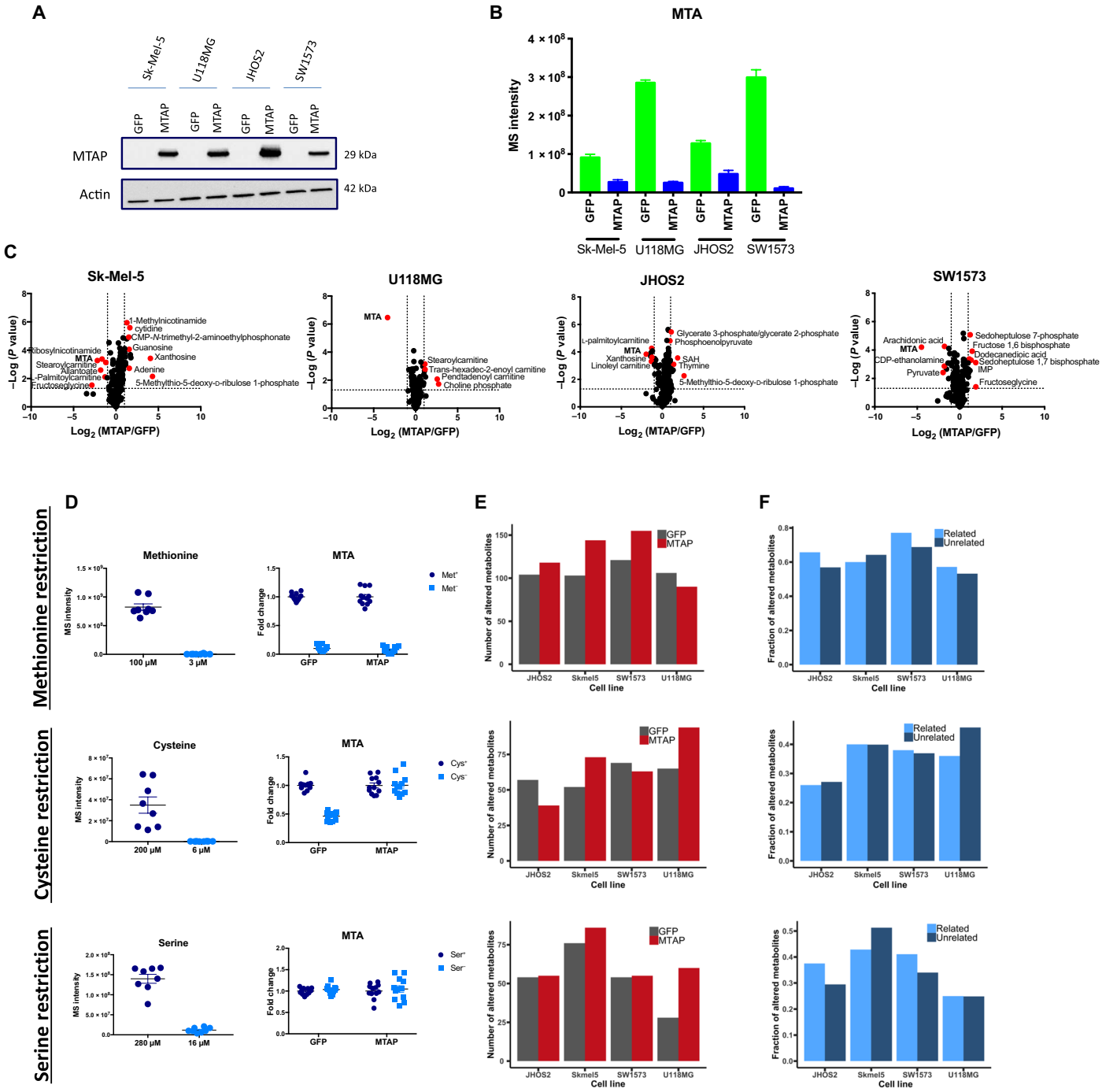

Fig. 4. Restoration of *MTAP* expression produces heterogeneous effects on metabolism. (**A**) Western blot validation of lentiviral ectopic expression of *MTAP* (compared to GFP control) in *MTAP*$^{-/-}$ cell lines. (**B**) Integrated intensity values of relative MTA metabolite levels in *MTAP*- or GFP-infected cell lines. (**C**) Volcano plots of each cell line, showing fold change values of metabolites between *MTAP*-infected and GFP-infected isogenic pairs. *P* values obtained using Student's *t* test. IMP, inosine 5′-monophosphate; CDP, cytidine 5′-diphosphate. (**D**) Validation of nutrient restriction using integrated intensity values of the respective nutrient (left) and fold change values of MTA metabolite levels in complete/restricted culture conditions (right). (**E**) Number of significantly altered ($P < 0.05$, Student's *t* test) metabolites in *MTAP*-expressing lines compared to GFP controls. (**F**) Fraction of significantly altered ($P < 0.05$, Student's *t* test) metabolites that are related (i.e., within five reactions) or unrelated to the indicated nutrient.

to control cells (Fig. 4B). The expression of *MTAP* in these cell lines resulted in changes to both global and methionine metabolism in each of the cell lines; however, only one metabolite (MTA) was significantly altered in all four lines (Fig. 4C).

Ectopic *MTAP* expression did not significantly affect responsiveness of MTA levels to methionine or serine restriction, although cysteine restriction resulted in a significant drop in MTA levels exclusively in *MTAP*$^{-/-}$ lines (Fig. 4D). *MTAP* reexpression also largely did not appear

to significantly alter overall responsiveness to methionine, cysteine, or serine availability compared to controls as evidenced both by the number of metabolites related to methionine (fig. S4A) and to the overall changes in metabolism (Fig. 4E and fig. S4B). In addition, *MTAP* reexpression also did not seem to increase the proportion of significantly altered metabolites that were related versus unrelated to the respective nutrient that was restricted (Fig. 4F). These results imply that while ectopic *MTAP* expression in *MTAP*-deleted cancer cell lines can induce significant metabolic alterations, these effects are not similar between cell lines and are not sufficient to override the programmed responsiveness to nutrient availability that has been adapted by individual cell lines.

MTAP status remains nonpredictive of responsiveness to nutrient restriction in a panel of tissue-matched cell lines

To further characterize how *MTAP* deletion affects one-carbon metabolism in a tissue-matched set of cell lines, we next examined a panel of seven brain-derived cancer cell lines (three $MTAP^{+/+}$ and four $MTAP^{-/-}$); the presence or the absence of *MTAP* protein was verified by immunoblotting (Fig. 5A), and *MTAP* and Cdkn2a transcript levels were validated using quantitative polymerase chain reaction (qPCR) (fig. S5A). Of note, as a result of the relative scarcity of p16/$MTAP^{+/+}$ glioma cell lines due to the high prevalence of p16 alterations in brain cancers (*9*), one of three $MTAP^{+/+}$ cell lines in this panel was determined to be p16 null (fig. S5A). Analysis of global metabolic profiles of these cell lines again identified MTA as the most differentially abundant metabolite (Fig. 5B), with cysteine and methionine metabolism being one of the most differential metabolic pathways between the two groups (Fig. 5C and table S2). PCA demonstrated that *MTAP* status only accounted for slightly more of the variation (7.7% in PC5) in the metabolic profiles of these cell lines (Fig. 5) than was found in our original panel (Fig. 1D).

We then conducted methionine (Fig. 5E), cysteine (Fig. 5F), and serine (Fig. 5G) restrictions for each cell line; consistent with our previous results, we found that these cell lines all responded to each nutrient restriction in a unique and heterogeneous manner and that these metabolic shifts were not primarily associated with *MTAP* status as evidenced by the clustering patterns of the resulting metabolic profiles (Fig. 5, E to G, and fig. S5B). Compared to our previous cell line panel, we found that methylated metabolites were more consistently altered by methionine restriction in these tissue-matched cell lines, independent of *MTAP* status (fig. S5B); furthermore, $MTAP^{+/+}$ cell lines exhibited less variable responsiveness and greater sensitivity to cysteine restriction (fig. S5B), supporting our previous observations that $MTAP^{-/-}$ cell lines tended to exhibit relatively less sensitivity to cysteine restriction within cysteine-related metabolic pathways (Fig. 3F).

Methionine restriction effectively reduced MTA levels in $MTAP^{-/-}$ cells to those found in $MTAP^{+/+}$ cells in methionine-rich culture conditions (Fig. 5H), while cysteine restriction significantly reduced MTA levels solely in $MTAP^{+/+}$ cells and serine restriction did not significantly alter MTA levels in any cell line (fig. S5D). However, we found that the fraction of methionine-related metabolites (Fig. 5I), as well as cysteine-related or serine-related (fig. S5E) metabolites, that were significantly altered by the respective nutrient restriction did not differ between $MTAP^{+/+}$ and $MTAP^{-/-}$ groups and, in most cell lines, was comparable to the fraction of significantly altered metabolites that were unrelated to the restricted nutrient. Last, PCA demonstrated that methionine restriction continued to account for more of the variance in global metabolic profiles compared to *MTAP* status (Fig. 5J and fig. S5E). Together, the results in this tissue-matched panel of brain-derived cell lines are in line with those found in the previous panel of tissue-variable cell lines and demonstrate that *MTAP* status is insufficient to shape how a given cell line will respond to alterations in the environment.

Of note, while linoleic acid metabolism was found to be significantly affected both between $MTAP^{+/+}$ and $MTAP^{-/-}$ groups (Fig. 1C) and upon each of the nutrient restrictions (Figs. 2B and 3B) in our panel of 10 cell lines originating from different tissues, this pathway was not found to be significantly affected upon nutrient restriction in this panel of brain-derived cell lines (Fig. 5C); upon further examination, we found that this was specifically due to alterations in linoleic acid (which is the central metabolite within this metabolic process and thus is highly weighted in the pathway analysis), while the other metabolites in this pathway were not significantly affected. Although the significance of this observation is presently unclear, this may represent a tissue-specific phenotype and provides an interesting avenue for future investigations of gene-environment interactions in the context of fatty acid metabolism.

Defining the quantitative impact of *MTAP* deletion and environmental factors on metabolism

These results thus far reveal that heterogeneity across cell types and nutrient availability exert dominant effects on metabolism relative to *MTAP* status. For example, each cell line exhibited marked differences in the number of altered metabolites in response to nutrient restriction independent of *MTAP* status or tissue identity (Fig. 6A). Furthermore, when the numbers of unique significantly altered metabolites were averaged within $MTAP^{+/+}$ and $MTAP^{-/-}$ groups, we found that the two groups displayed similar degrees of responsivity to methionine restriction, while the $MTAP^{+/+}$ cell lines were, on average, more responsive to serine and cysteine restriction (Fig. 6B), as was further confirmed using three independent statistical analyses (Student's *t*, Kruskal-Wallis, and Mann-Whitney *U* tests) (Fig. 6C). An additional comparison of the number of altered metabolites between $MTAP^{+/+}$ and $MTAP^{-/-}$ cell lines demonstrated that each nutrient restriction had a substantially greater impact on global metabolism than *MTAP* deletion by itself (Fig. 6D).

As cancer cell lines are known to individually exhibit a unique combination of both genetic and environmentally driven transcriptional programs, and that previous studies suggest that *MTAP* deletion may elicit epigenetic consequences (*9*, *10*), we next sought to determine whether the *MTAP*-deleted cell lines included in our panel exhibit differential expression of other enzymes involved in one-carbon metabolism compared to *MTAP*-expressing cell lines. Upon analysis of RNA sequencing data (*29*), we found that although we correctly predicted that the expression of these metabolic enzymes is highly variable between cell lines (fig. S6A), this variability is comparable within $MTAP^{+/+}$ and $MTAP^{-/-}$ groups and is thus not likely to be the determinant of the observed metabolic differences between the two groups. Furthermore, Spearman rank correlations generated from full RNA sequencing datasets demonstrate that these cell lines do not cluster by either *MTAP* status or tissue type, consistent with the results of our metabolomics analysis (fig. S6B).

To quantify the relative contribution of *MTAP* deletion and the availability of each nutrient, we developed a machine-learning classifier with a support vector machine using the top 100 metabolites exhibiting the highest SD within each restriction dataset (Fig. 6E and Methods). First, a PCA was used to generate a vector that accounts for 70% of the variation across all of the samples. This

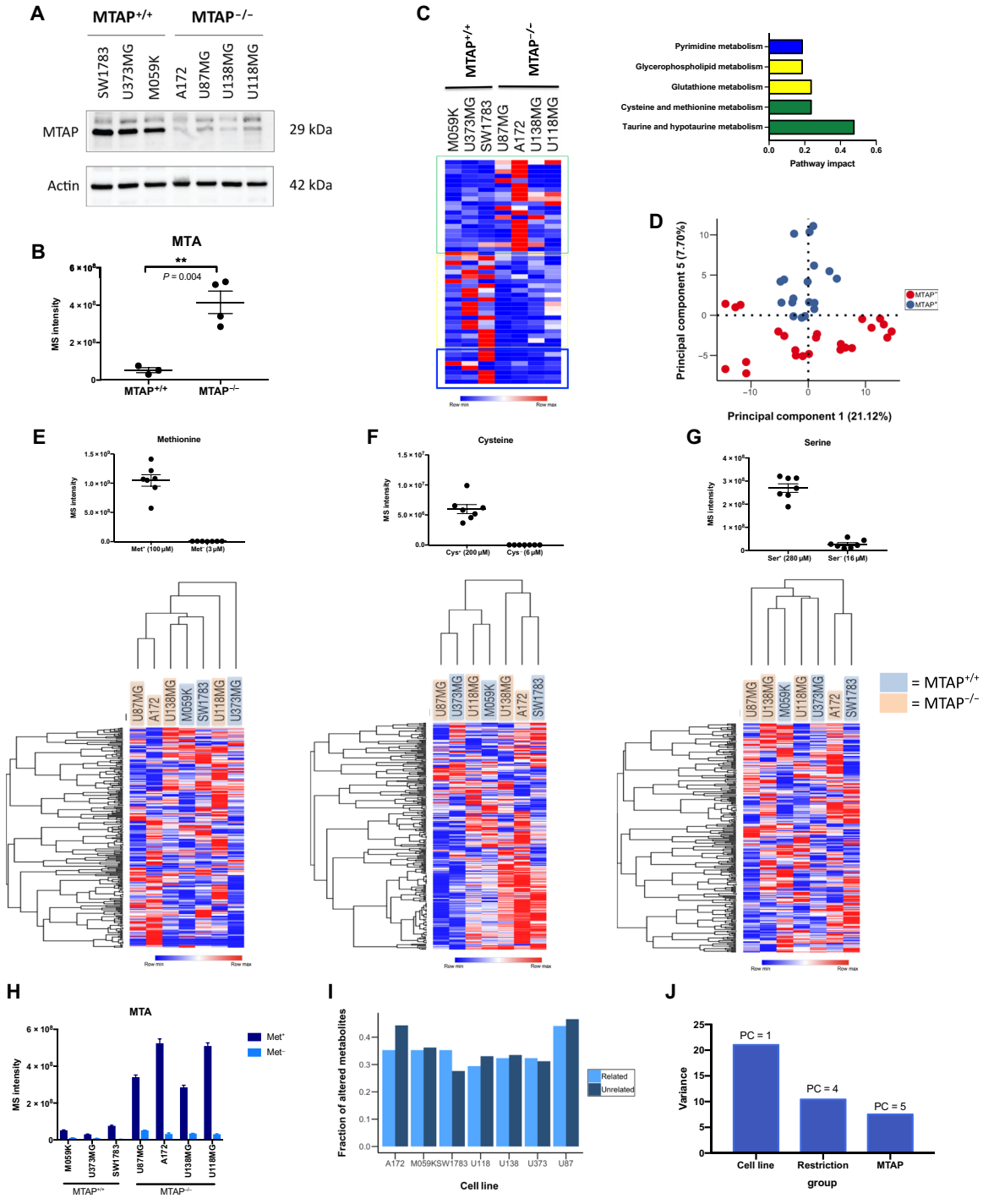

Fig. 5. *MTAP* status remains nonpredictive of responsiveness to nutrient restriction in a panel of tissue-matched cell lines. (**A**) Western blot validation of *MTAP* expression. (**B**) Relative metabolite abundance of MTA in $MTAP^{+/+}$ versus $MTAP^{-/-}$ cell lines. *P* values were obtained from Student's *t* test. (**C**) Heat map of top 50 differential metabolites between $MTAP^{+/+}$ and $MTAP^{-/-}$ cell lines. Top affected pathways are indicated. (**D**) PCA of variance between $MTAP^{+/+}$ and $MTAP^{-/-}$ groups. (**E** to **G**) Relative metabolite abundance of (E) methionine, (F) cysteine, and (G) serine and the resulting heat maps of global metabolic profiles generated in each cell line from the indicated nutrient restriction. (**H**) Relative metabolite abundance of MTA in cell lines cultured in complete or methionine-restricted medium. (**I**) Fraction of significantly altered ($P < 0.05$, Student's *t* test) metabolites that are related (i.e., within five reactions) or unrelated to methionine. (**J**) Assignment of PC that displays greatest variance between the indicated groups.

classifier was tested for its ability to discriminate (for both sensitivity and specificity) *MTAP* status or nutrient (cysteine, methionine, or serine) availability. In each case of differential nutrient availability, the nutrient status outperformed *MTAP* status in accounting for the variation across the data. Thus, these collective results demonstrate that while *MTAP* deletion does confer a reproducible metabolic signature within a single environment, the availability of nutrients related to *MTAP* (i.e., methionine, serine, and cysteine) has a larger

A

Number of altered metabolites ($P < 0.05$)

Restriction	Calu6	SW1573	HT1197	RT4	Ov90	JHOS2	UACC257	Skmel5	M059K	U118MG
Methionine	27	110	26	30	35	24	22	12	69	15
Serine	94	20	37	35	72	32	27	36	31	26
Cysteine	80	68	38	45	62	49	80	28	74	55

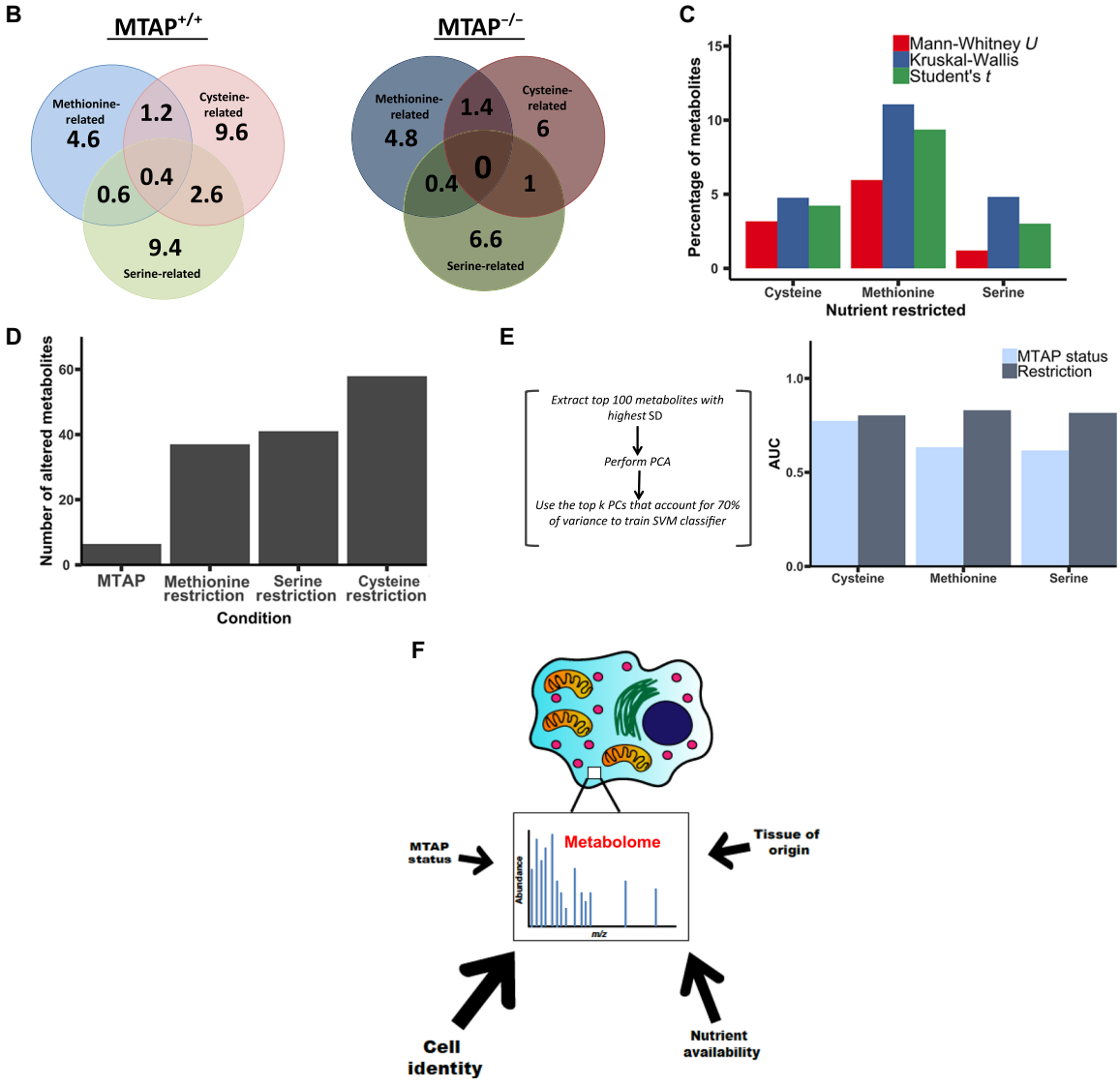

Fig. 6. Integration of responsiveness to nutrient restriction determines quantitative impact of *MTAP* deletion on global metabolic networks. (**A**) Number of significantly altered ($P < 0.05$, Student's *t* test) metabolites for each cell line under each of the three nutrient restriction conditions. (**B**) Venn diagrams depicting overlap of average number of significantly altered related metabolites within a cell line for $MTAP^{+/+}$ and $MTAP^{-/-}$ groups. (**C**) Number of significantly altered metabolites for each nutrient restriction, as determined by three separate statistical analyses as indicated. (**D**) Number of total unique significantly altered metabolites for each condition indicated. (**E**) AUC of top PCs that account for 70% of variance between either $MTAP^{+/+}$ and $MTAP^{-/-}$ or control and restricted nutrient conditions. (**F**) Graphical summary illustrating that environment and cell identity shape the metabolome to a greater extent than *MTAP* status or tissue of origin.

effect both on *MTAP*-related methionine metabolism and on the global metabolic network, which is further confounded by metabolic variation across cell lines that span different tissues of origin (Fig. 6F).

DISCUSSION

Cells have been thought to exhibit similar metabolic phenotypes based on their genetic status (*30*–*33*). In line with this, it has recently been proposed that *MTAP* deletion creates a state of disordered

methionine metabolism resulting in targetable liabilities, in both metabolism and the epigenetic regulation that is connected to methionine metabolism (*8*–*10*, *15*, *34*). It has also become increasingly appreciated that environmental factors can markedly influence the status of metabolism (*35*, *36*); for example, it was recently shown that the same tumorigenic genetic event, when initiated in different tissues, results in different metabolic programs and requirements (*22*). Therefore, while the proposed liabilities induced by *MTAP* deletion may be promising, this study reveals that methionine metabolism can be shaped by environmental factors outside, thus supporting the conclusion that contextual factors beyond a single genetic event should be considered when characterizing metabolism. Using *MTAP* status and the pathway, its enzyme resides in (i.e., methionine and, by extension, one-carbon metabolism) as a model to quantitatively and systematically study the relevant variables that shape metabolic outcomes, we found that while perhaps expectedly global metabolism was not overall predictive of *MTAP* status, methionine metabolism as well was also shaped to a greater extent by the nutrients that are used in the one-carbon network and by cell-to-cell variability.

Our results demonstrate that while metabolic signatures of *MTAP* status across diverse cell types are reproducible in nutrient-rich culture medium, these signatures are lost upon consideration of nutrient availability. For instance, we found that the accumulation of MTA, which was essential for mediating the collateral lethality induced by *MTAP* deletion (*8*–*10*), was abrogated when cells were subjected to methionine or cysteine restriction. Furthermore, metabolic variation in one-carbon metabolism across cell types was far greater than the differences observed in a pan tissue analysis of *MTAP* wild-type and homozygous deleted cells; unexpectedly, each cell type exhibited markedly different metabolic outcomes upon nutrient restriction, which were not predicted by *MTAP* status. In addition, reexpression of functional *MTAP* protein produced extremely heterogeneous consequences on various metabolic pathways beyond methionine metabolism across a diverse panel of cell lines. Nevertheless, these results by no means exclude the possibility of targeting methionine metabolism (or *MTAP*-deleted cancers) by, for example, inhibiting MAT2a but instead further illustrate the complexities of gene-environment interactions that may influence the efficacy of therapeutic approaches in highly variable patient populations.

Considering that many studies of metabolism are conducted in nutrient-rich media designed for optimal cell proliferation or protein production (which can exhibit methionine concentrations up to threefold higher than of those found in human plasma) and that tissues exhibit substantially variable metabolic requirements and nutrient availabilities in a physiological setting (*22*), our results contribute to our understanding of the limitations inherent to current experimental approaches using cell culture; it will therefore be essential in future investigations to consider how dietary nutrient composition may influence genetically driven phenotypes, particularly in a physiological setting. Other examples of collateral lethality that depend on genetically defined altered metabolisms in general, such as the case of malic enzyme or enolase (*37*, *38*), may likely encounter similar considerations. Together, these findings indicate greater complexities in the factors that shape metabolism beyond individual genetic alterations.

METHODS

Cell culture

Cells were cultured at 37°C, with 5% atmospheric CO_2 in RPMI 1640 (Gibco), 10% heat-inactivated fetal bovine serum (FBS), penicillin (100 U/ml), and streptomycin (100 mg/ml). All cell lines were obtained from the American Tissue Culture Collection except UACC-257 (obtained from the National Cancer Institute, National Institutes of Health), U373MG (obtained from the Duke Cell Culture Facility), and JHOS2 (obtained from A. Berchuck, Duke University).

Nutrient restriction

For all nutrient restriction experiments, cells were plated at a density of 3×10^5 cells per well in triplicate in a six-well plate and were allowed to adhere for 24 hours. Conditional medium was prepared using RPMI 1640 lacking amino acids, glucose, and glutamine. Dropout medium (i.e., Met^-, Ser^-, or Cys^-) was supplemented with 5 mM glucose, 2 mM glutamine, 10% heat-inactivated FBS, penicillin (100 U/ml), streptomycin (100 mg/ml), and 19 of 20 individual amino acids (excluding either methionine, serine, or cystine) at concentrations found in full RPMI 1640 medium. For full media conditions in these experiments, the respective nutrient of interest was individually added back to the medium (i.e., Met^+, Ser^+, or Cys^+). For all experiments, three technical replicates per culture condition for each cell line were used.

Cell viability assays

For all cell viability measurements, cells were plated at a density of 5×10^3 cells per well in triplicate in a 96-well plate and were allowed to adhere in full RPMI 1640 medium for 24 hours. Conditional medium, containing four (serine) or five (cystine or methionine) increasing concentrations of the respective nutrient, was prepared as previously described. After 24 hours, cells were briefly washed with phosphate-buffered saline (PBS) and then incubated in the conditional medium for 24 hours. After 24 hours, the medium was aspirated and replaced with 100 μl phenol red–free RPMI 1640 (Gibco) and 12 mM 3-[4,5-dimethylthiazol-2-yl]-2,5-diphenyltetrazolium (MTT) (no. M6494, Thermo Fisher Scientific). After 4 hours, the MTT-containing medium was aspirated, and 50-μl dimethyl sulfoxide was added to dissolve the formazan. After 5 min, absorbance was read at 540 nm.

Lentiviral transfection and transduction

Human embryonic kidney 293T cells were plated at a density of 1×10^6 cells/10 cm plate in RPMI 1640 (Gibco) supplemented with 10% heat-inactivated FBS, penicillin (100 U/ml), and streptomycin (100 mg/ml) and were allowed to adhere and reach 70% confluency. Fifteen micrograms of *MTAP* (EX-A3221-Lv105, GeneCopoeia) or GFP control (EX-EGFP-Lv105, GeneCopoeia) plasmid, 10 μg of PsPAX2 packaging vector (no. 12260, Addgene), and 5 μg of PMD2. G envelope–expressing plasmids (no. 12259, Addgene) were diluted in 500 μl of jetPRIME buffer (no. 114-07, Polyplus-transfection) and vortexed. Next, 60 μl of the jetPRIME transfection reagent (no. 114-07, Polyplus-transfection) was added to the mixture, vortexed for 10 s, and left to incubate for 10 min at room temperature. The medium in the plate was replaced with fresh medium, and the transfection mix was then added to the 10-cm plate dropwise. After 24 hours, the transfection medium was replaced with fresh medium. After an additional 24 hours, the medium was collected and filtered through a 0.45-μm filter for virus collection. SW1573, U118MG, JHOS2, and Sk-Mel-5 cells were plated in 10-cm plates, and when they reached 30 to 50% confluency, virus-containing medium (1:1 with fresh RPMI 1640 medium) was added to the plates, along with polybrene (4 μg/μl). After 24 hours, the virus-containing medium was removed and replaced with fresh RPMI 1640 medium. Cells were incubated with puromycin (1 μg/ml) for 48 hours, and

MTAP expression in the four isogenic cell pairs (eight lines total) were verified by immunoblotting.

Immunoblotting

Samples were homogenized in 100 µl of 1× radioimmunoprecipitation assay buffer (VWR International) supplemented with 100 µM phenylmethylsulfonyl fluoride, aprotinin (2 µg/µl), 1× phosphatase inhibitor cocktail, and 2 mM dithiotheritol. Cell lysates were centrifuged at 14,000 rpm for 30 min at 4°C. The resulting supernatant was transferred to a clean tube, and a bicinchoninic acid assay (Thermo Fisher Scientific) was carried out to quantify protein concentration. Protein samples were loaded onto TGX Stain-Free precast gels (Bio-Rad) and transferred to polyvinylidene difluoride membranes. Membranes were blocked in 5% dry nonfat milk in either tris-buffered or phosphate-buffered saline with 0.1% Tween-20 (TBST or PBST, respectively) and incubated in anti-*MTAP* [1:7500 (Figs. 1B and 4A), 1:1333 (Fig. 5A) in 5% BSA in TBST; no. 4158S, Cell Signaling] and anti-actin [1:2000 (Figs. 1B and 4A) and 1:1000 (Fig. 5A) in 5% dry nonfat milk in TBST/PBST; no. MA5-15739, Thermo Fisher Scientific] overnight at 4°C. Membranes were washed three times for 10 min (Figs. 1B and 4A) or 5 min (Fig. 5A) each with TBST/PBST. Horseradish peroxidase–conjugated anti-mouse (no. 610-1302, Rockland) and anti-rabbit (no. 611-1302, Rockland), both 1:2000 (Figs. 1B and 4A) or 1:3000 (Fig. 5A), were used as secondary antibodies in 5% dry nonfat milk in TBST/PBST at room temperature for 20 min (Figs. 1B and 4A) or 60 min (Fig. 5A). Membranes were washed three times in TBST/PBST once more, and then chemiluminescent signals were detected with the Clarity Western ECL Detection Kit (no. 1705061, Bio-Rad) (Figs. 1B and 4A) or SuperSignal West Pico PLUS Chemiluminescent Substrate (no. 34579, Thermo Fisher Scientific) (Fig. 5A). The membranes were then imaged using the ChemiDoc Touch Imaging System (Bio-Rad).

Quantitative PCR

Confluent 10-cm^2 plates of each cell line were washed with ice-cold PBS, and 1 ml of TRIzol (no. 15596026, Amibon by Life Technologies) was added to each plate. Cells were scraped into the TRIzol solution and transferred to tubes. Chloroform (200 µl) was then added to each tube, and samples were briefly vortexed and then incubated at room temperature for 3 min. Samples were then centrifuged at 12,000*g* at 4°C for 15 min. The clear upper aqueous layer was transferred to a fresh tube, and 500-µl isopropanol was added to precipitate RNA. The samples were incubated at room temperature for 10 min and then centrifuged at 12,000*g* at 4°C for 10 min. The supernatant was removed, and the RNA pellet was washed twice with 1 ml of 75% ethanol; between and after washes, samples were vortexed and then centrifuged at 7500*g* at 4°C for 5 min. The resulting RNA pellets were then air-dried for 10 min and resuspended in 100 µl of nuclease-free water. RNA quantity/quality was assessed by NanoDrop Spectrophotometer measurements using a Bioanalyzer 2100 (Agilent Technologies). One microgram of total RNA was then converted to single-strand complementary DNA using the Reverse Transcription System (no. A3500, Promega). Expression levels of Cdkn2a, *MTAP*, and 18-S transcripts were assessed by qPCR on a CFX384 Touch Real-Time PCR Detection System (Bio-Rad) using iTaq Universal SYBR Green (Bio-Rad) and the following primers (Integrated DNA Technologies): Cdkn2a-forward (5′-TGTGCCACACATCTTTGACCT-3′) and Cdkn2a-reverse (5′-AGGACCTTCGGTGACTGATGA-3′); *MTAP*-forward (5′-TGGAATAATTGGTGGAACAGGC-3′) and *MTAP*-reverse (5′-TGGCACACTCCTCTGGCAC-3′); and 18-S–forward (5′-CTTAGAGGGACAAGTGGCG-3′) and 18-S–reverse (5′-ACGCTGAGCCAGTCAGTGTA-3′). Samples were run in three technical replicates. The difference between the highest and lowest quantification cycles (dCq) values for Cdkn2a and *MTAP* were calculated as follows: $2^{-[Cq(Cdkn2a \text{ or } MTAP) - Cq(18S)]}$. Data were plotted as (mean dCq ± SEM) × 10^7.

Metabolite extraction

Medium was quickly aspirated, and 1 ml of extraction solvent (80% methanol/water, cooled to −80°C) was added to each well of the six-well plates, which were then transferred to −80°C for 15 min. Plates were removed, and cells were scraped into the extraction solvent on dry ice. All metabolite extracts were centrifuged at 20,000*g* at 4°C for 10 min. Last, the solvent in each sample was evaporated in a speed vacuum, and the resulting pellets were stored in −80°C until resuspension. For polar metabolite analysis, the cell extract was dissolved in 15 µl of water and 15 µl of methanol/acetonitrile (1:1, v/v) [liquid chromatography–mass spectrometry (LC-MS) optima grade, Thermo Fisher Scientific]. Samples were centrifuged at 20,000*g* for 2 min at 4°C, and the supernatants were transferred to LC vials.

Liquid chromatography

UltiMate 3000 HPLC (Dionex) with an XBridge Amide column [100 mm × 2.1 mm inner diameter (i.d.), 3.5 µm; Waters] was coupled to a Q Exactive (QE) mass spectrometer (Thermo Fisher Scientific) for metabolite separation and detection at room temperature. The mobile phase A reagent was composed of 20 mM ammonium acetate and 15 mM ammonium hydroxide in 3% acetonitrile in high-performance liquid chromatography (HPLC)–grade water (pH 9.0), while the mobile phase B reagent was acetonitrile. All solvents were of LC-MS grade, purchased from Thermo Fisher Scientific. The flow rate used was 0.15 ml/min from 0 to 10 min and 15 to 20 min, and 0.3 ml/min from 10.5 to 14.5 min. The linear gradient was as follows: 0 min 85% B, 1.5 min 85% B, 5.5 min 35% B, 10 min 35% B, 10.5 min 25% B, 14.5 min 35% B, 15 min 85% B, and 20 min 85% B.

Mass spectrometry

The QE mass spectrometer (Thermo Fisher Scientific) was outfitted with a heated electrospray ionization probe (HESI) with the following parameters: evaporation temperature, 120°C; sheath gas, 30; auxiliary gas, 10; sweep gas, 3; and spray voltage, 3.6 kV for positive mode and 2.5 kV for negative mode. Capillary temperature was set at 320°C, and S-lens was 55. A full scan range was set at 60 to 900 mass/charge ratio (*m*/*z*) with the resolution set to 70,000. The maximum injection time was 200 ms. Automated gain control was targeted at 3 million ions.

Peak extraction and metabolomics data analysis

Data collected from LC-QE mass spectrometer was processed using commercially available software Sieve 2.0 (Thermo Fisher Scientific). For targeted metabolite analysis, the method "peak alignment and frame extraction" was applied. An input file ("frame seed") of theoretical *m*/*z* (width set at 10 ppm) and retention time of ~260 known metabolites were used for positive mode analysis, while a separate frame seed file of ~200 metabolites was used for negative mode analysis. To calculate the fold changes between different experimental groups, integrated peak intensities generated from the raw data were used. Hierarchical clustering and heat maps were generated using Morpheus software (Broad Institute, https://software.broadinstitute.org/morpheus/). For hierarchical clustering, Spearman correlation parameters were implemented for row and column parameters. Pathway enrichment analysis was conducted using MetaboAnalyst

3.0 software (www.metaboanalyst.ca/faces/home.xhtml); briefly, metabolite identifications from the human metabolome database (HMDB IDs) from the metabolites that were significantly enriched [greater than $\log_2$ (fold change) with $P < 0.05$] were inputted. The pathway library used was *Homo sapiens* and Fisher's exact test was used for over-representation analysis. Other quantitation and statistics were calculated using GraphPad Prism software.

Statistical analysis

For the control data from the three nutrient restriction experiments, raw intensities of metabolites were log-transformed [$\log_{10}(x + 1)$], corrected for batch effect using the removeBatchEffect() function in the LIMMA R package (*39*), and then *z* score normalized. Other metabolomic data and fold changes between conditions were also *z* score normalized before the following analysis. PCA was performed using the PCA() function from the FactoMineR R package (*40*). Correlation (r^2) between each PC and each of the three categorical variables (*MTAP* status, Cell Line, and Tissue of Origin) was also calculated by the PCA() function from FactoMineR. Analysis of variance (ANOVA) was done on each of the three categorical variables and the first 10 PCs using the aov() function in R. Unpaired Student's *t* test was used for comparison between two groups unless otherwise stated. A *P* value <0.05 was considered as statistically significant.

Machine learning

The area under the curve (AUC) of the receiver operating characteristic curve was computed using the perfcurve() function in MATLAB. Classification was done using the MATLAB Classification Learner App. Briefly, for binary classification of *MTAP* status or nutrient status based on metabolite abundances, the top 100 metabolites with the highest SD in their raw intensities were kept. Average intensities from three replicates were *z* score normalized and then subjected to PCA with the pca() function in MATLAB. The minimal number of PCs that accounted for at least 70% of the variance was used to train the linear support vector machine (SVM) model for the classification. The AUC was calculated using fivefold cross-validation.

Network analysis

The genome-scale reconstruction of human metabolism, Recon2 (*41*), was used as the metabolic network model in defining the nutrient-related and nutrient-unrelated metabolites. Metabolites that were five or fewer reactions away from the nutrient (methionine, serine, or cysteine) were categorized as "related"; otherwise, they were categorized as "unrelated." Only enzyme-catalyzed reactions with the highest confidence score were considered. Cofactors associated with more than 100 reactions were also excluded from the analysis.

SUPPLEMENTARY MATERIALS

Supplementary material for this article is available at http://advances.sciencemag.org/cgi/content/full/5/6/eaav7769/DC1

Fig. S1. Cancer cell lines exhibiting homozygous codeletions of p16/*MTAP* show altered patterns of metabolite levels.

Fig. S2. Responsiveness to methionine availability is not predicted by *MTAP* status.

Fig. S3. Responsiveness to alterations in other one-carbon nutrient availability is largely *MTAP* status independent.

Fig. S4. Restoration of *MTAP* expression produces heterogeneous effects on metabolism.

Fig. S5. *MTAP* status remains nonpredictive of responsiveness to nutrient restriction in a panel of tissue-matched cell lines.

Fig. S6. Gene expression does not strongly correlate with *MTAP* status or originating tissue in panel of 10 cell lines.

Table S1. Top 50 differential metabolites between $MTAP^{+/+}$ and $MTAP^{-/-}$ cell lines.

Table S2. Top 50 differential metabolites between $MTAP^{+/+}$ and $MTAP^{-/-}$ glioma cell lines.

REFERENCES AND NOTES

1. R. Beroukhim, C. H. Mermel, D. Porter, G. Wei, S. Raychaudhuri, J. Donovan, J. Barretina, J. S. Boehm, J. Dobson, M. Urashima, K. T. Mc Henry, R. M. Pinchback, A. H. Ligon, Y.-J. Cho, L. Haery, H. Greulich, M. Reich, W. Winckler, M. S. Lawrence, B. A. Weir, K. E. Tanaka, D. Y. Chiang, A. J. Bass, A. Loo, C. Hoffman, J. Prensner, T. Liefeld, Q. Gao, D. Yecies, S. Signoretti, E. Maher, F. J. Kaye, H. Sasaki, J. E. Tepper, J. A. Fletcher, J. Tabernero, J. Baselga, M.-S. Tsao, F. Demichelis, M. A. Rubin, P. A. Janne, M. J. Daly, C. Nucera, R. L. Levine, B. L. Ebert, S. Gabriel, A. K. Rustgi, C. R. Antonescu, M. Ladanyi, A. Letai, L. A. Garraway, M. Loda, D. G. Beer, L. D. True, A. Okamoto, S. L. Pomeroy, S. Singer, T. R. Golub, E. S. Lander, G. Getz, W. R. Sellers, M. Meyerson, The landscape of somatic copy-number alteration across human cancers. *Nature* **463**, 899–905 (2010).
2. H. Zhang, Z.-H. Chen, T. M. Savarese, Codeletion of the genes for $p16^{INK4}$, methylthioadenosine phosphorylase, interferon-α1, interferon-β1, and other 9p21 markers in human malignant cell lines. *Cancer Genet. Cytogenet.* **86**, 22–28 (1996).
3. M. Lubin, A. Lubin, Selective killing of tumors deficient in methylthioadenosine phosphorylase: A novel strategy. *PLOS ONE* **4**, e5735 (2009).
4. B. Tang, Y. Kadariya, Y. Chen, M. Slifker, W. D. Kruger, Expression of *MTAP* inhibits tumor-related phenotypes in HT1080 cells via a mechanism unrelated to its enzymatic function. *G3* **5**, 35–44 (2014).
5. S. F. V. de Oliveira, M. Ganzinelli, R. Chilà, L. Serino, M. E. Maciel, C. de Andrade Urban, R. S. de Lima, I. J. Cavalli, D. Generali, M. Broggini, G. Damia, E. M. de Souza Fonseca Ribeiro, Characterization of *MTAP* gene expression in breast cancer patients and cell lines. *PLOS ONE* **11**, e0145647 (2016).
6. Z.-H. Chen, O. I. Olopade, T. M. Savarese, Expression of methylthioadenosine phosphorylase cDNA in*p16-*, *MTAP-* malignant cells: Restoration of methylthioadenosine phosphorylase-dependent salvage pathways and alterations of sensitivity to inhibitors of purine de novo synthesis. *Mol. Pharmacol.* **52**, 903–911 (1997).
7. A. L. Subhi, P. Diegelman, C. W. Porter, B. Tang, Z. J. Lu, G. D. Markham, W. D. Kruger, Methylthioadenosine phosphorylase regulates ornithine decarboxylase by production of downstream metabolites. *J. Biol. Chem.* **278**, 49868–49873 (2003).
8. K. Marjon, M. J. Cameron, P. Quang, M. F. Clasquin, E. Mandley, K. Kunii, M. McVay, S. Choe, A. Kernytsky, S. Gross, Z. Konteatis, J. Murtie, M. L. Blake, J. Travins, M. Dorsch, S. A. Biller, K. M. Marks, *MTAP* deletions in cancer create vulnerability to targeting of the MAT2A/PRMT5/RIOK1 axis. *Cell Rep.* **15**, 574–587 (2016).
9. G. V. Kryukov, F. H. Wilson, J. R. Ruth, J. Paulk, A. Tsherniak, S. E. Marlow, F. Vazquez, B. A. Weir, M. E. Fitzgerald, M. Tanaka, C. M. Bielski, J. M. Scott, C. Dennis, G. S. Cowley, J. S. Boehm, D. E. Root, T. R. Golub, C. B. Clish, J. E. Bradner, W. C. Hahn, L. A. Garraway, *MTAP* deletion confers enhanced dependency on the PRMT5 arginine methyltransferase in cancer cells. *Science* **351**, 1214–1218 (2016).
10. K. J. Mavrakis, E. R. McDonald III, M. R. Schlabach, E. Billy, G. R. Hoffman, A. deWeck, D. A. Ruddy, K. Venkatesan, J. Yu, G. McAllister, M. Stump, R. deBeaumont, S. Ho, Y. Yue, Y. Liu, Y. Yan-Neale, G. Yang, F. Lin, H. Yin, H. Gao, D. R. Kipp, S. Zhao, J. T. McNamara, E. R. Sprague, B. Zheng, Y. Lin, Y. S. Cho, J. Gu, K. Crawford, D. Ciccone, A. C. Vitari, A. Lai, V. Capka, K. Hurov, J. A. Porter, J. Tallarico, C. Mickanin, E. Lees, R. Pagliarini, N. Keen, T. Schmelzle, F. Hofmann, F. Stegmeier, W. R. Sellers, Disordered methionine metabolism in *MTAP*/CDKN2A-deleted cancers leads to dependence on PRMT5. *Science* **351**, 1208–1213 (2016).
11. J. W. Locasale, Serine, glycine and one-carbon units: cancer metabolism in full circle. *Nat. Rev. Cancer* **13**, 572–583 (2013).
12. M. Yang, K. H. Vousden, Serine and one-carbon metabolism in cancer. *Nat. Rev. Cancer* **16**, 650–662 (2016).
13. A. C. Newman, O. D. K. Maddocks, One-carbon metabolism in cancer. *Br. J. Cancer* **116**, 1499–1504 (2017).
14. G. S. Ducker, J. D. Rabinowitz, One-carbon metabolism in health and disease. *Cell Metab.* **25**, 27–42 (2017).
15. S. J. Mentch, M. Merhmohamadi, L. Huang, X. Liu, D. Gupta, D. Mattocks, P. Gomez, G. Ables, M. M. Bamman, A. E. Thalacker-Mercer, S. Nichenametla, J. W. Locasale, Histone methylation dynamics and gene regulation occur through the sensing of one-carbon metabolism. *Cell Metab.* **22**, 861–873 (2015).
16. M. Mehrmohamadi, X. Liu, A. A. Shestov, J. W. Locasale, Characterization of the usage of the serine metabolic network in human cancer. *Cell Rep.* **9**, 1507–1519 (2014).
17. F. Kottakis, B. N. Nicolay, A. Roumane, R. Karnik, H. Gu, J. M. Nagle, M. Boukhali, M. C. Hayward, Y. Y. Li, T. Chen, M. Liesa, P. S. Hammerman, K. K. Wong, D. N. Hayes, O. S. Shirihai, N. J. Dyson, W. Haas, A. Meissner, N. Bardeesy, LKB1 loss links serine metabolism to DNA methylation and tumorigenesis. *Nature* **539**, 390–395 (2016).

18. O. D. K. Maddocks, C. F. Labuschagne, P. D. Adams, K. H. Vousden, Serine metabolism supports the methionine cycle and DNA/RNA methylation through de novo ATP synthesis in cancer cells. *Mol. Cell* **61**, 210–221 (2016).
19. P. M. Tedeschi, E. K. Markert, M. Gounder, H. Lin, D. Dvorzhinski, S. C. Dolfi, L. L.-Y. Chan, J. Qiu, R. S. DiPaola, K. M. Hirshfield, L. G. Boros, J. R. Bertino, Z. N. Oltvai, A. Vazquez, Contribution of serine, folate and glycine metabolism to the ATP, NADPH and purine requirements of cancer cells. *Cell Death Dis.* **4**, e877 (2013).
20. O. D. K. Maddocks, C. R. Berkers, S. M. Mason, L. Zheng, K. Blyth, E. Gottlieb, K. H. Vousden, Serine starvation induces stress and p53-dependent metabolic remodelling in cancer cells. *Nature* **493**, 542–546 (2013).
21. O. D. K. Maddocks, D. Athineos, E. C. Cheung, P. Lee, T. Zhang, N. J. F. van den Broek, G. M. Mackay, C. F. Labuschagne, D. Gay, F. Kruiswijk, J. Blagih, D. F. Vincent, K. J. Campbell, F. Ceteci, O. J. Sansom, K. Blyth, K. H. Vousden, Modulating the therapeutic response of tumours to dietary serine and glycine starvation. *Nature* **544**, 372–376 (2017).
22. J. R. Mayers, M. E. Torrence, L. V. Danai, T. Papagiannakopoulos, S. M. Davidson, M. R. Bauer, A. N. Lau, B. W. Ji, P. D. Dixit, A. M. Hosios, A. Muir, C. R. Chin, E. Freinkman, T. Jacks, B. M. Wolpin, D. Vitkup, M. G. Vander Heiden, Tissue of origin dictates branched-chain amino acid metabolism in mutant Kras-driven cancers. *Science* **353**, 1161–1165 (2016).
23. M. O. Yuneva, T. W. M. Fan, T. D. Allen, R. M. Higashi, D. V. Ferraris, T. Tsukamoto, J. M. Matés, F. J. Alonso, C. Wang, Y. Seo, X. Chen, J. M. Bishop, The metabolic profile of tumors depends on both the responsible genetic lesion and tissue type. *Cell Metab.* **15**, 157–170 (2012).
24. X. Liu, Z. Ser, A. A. Cluntun, S. J. Mentch, J. W. Locasale, A strategy for sensitive, large scale quantitative metabolomics. *J. Vis. Exp.* **2014**, 52294 (2014).
25. X. Liu, Z. Ser, J. W. Locasale, Development and quantitative evaluation of a high-resolution metabolomics technology. *Anal. Chem.* **86**, 2175–2184 (2014).
26. X. Liu, J. W. Locasale, Metabolomics: A Primer. *Trends Biochem. Sci.* **42**, 274–284 (2017).
27. X. Gao, K. Lee, M. A. Reid, S. M. Sanderson, C. Qiu, S. Li, J. Liu, J. W. Locasale, Serine availability influences mitochondrial dynamics and function through lipid metabolism. *Cell Rep.* **22**, 3507–3520 (2018).
28. A. Muir, L. V. Danai, D. Y. Gui, C. Y. Waingarten, C. A. Lewis, M. G. V. Heiden, Environmental cystine drives glutamine anaplerosis and sensitizes cancer cells to glutaminase inhibition. *eLife* **6**, e27713 (2017).
29. R. Petryszak, M. Keays, Y. A. Tang, N. A. Fonseca, E. Barrera, T. Burdett, A. Füllgrabe, A. M.-P. Fuentes, S. Jupp, S. Koskinen, O. Mannion, L. Huerta, K. Megy, C. Snow, E. Williams, M. Barzine, E. Hastings, H. Weisser, J. Wright, P. Jaiswal, W. Huber, J. Choudhary, H. E. Parkinson, A. Brazma, Expression Atlas update—An integrated database of gene and protein expression in humans, animals and plants. *Nucleic Acids Res.* **44**, D746–D752 (2016).
30. M. G. Vander Heiden, L. C. Cantley, C. B. Thompson, Understanding the Warburg effect: the metabolic requirements of cell proliferation. *Science* **324**, 1029–1033 (2009).
31. A. Nagarajan, P. Malvi, N. Wajapeyee, Oncogene-directed alterations in cancer cell metabolism. *Trends Cancer* **2**, 365–377 (2016).
32. C. Commisso, S. M. Davidson, R. G. Soydaner-Azeloglu, S. J. Parker, J. J. Kamphorst, S. Hackett, E. Grabocka, M. Nofal, J. A. Drebin, C. B. Thompson, J. D. Rabinowitz, C. M. Metallo, M. G. Vander Heiden, D. Bar-Sagi, Macropinocytosis of protein is an amino acid supply route in Ras-transformed cells. *Nature* **497**, 633–637 (2013).
33. L. Li, L. Zhao, L. Li, J. Wu, M. Zhao, W. Du, L. Yu, P. Jiang, p53 regulation of ammonia metabolism through urea cycle controls polyamine biosynthesis. *Nature*, 1476–4687 (2019).
34. M. A. Reid, Z. Dai, J. W. Locasale, The impact of cellular metabolism on chromatin dynamics and epigenetics. *Nat. Cell Biol.* **19**, 1298–1306 (2017).
35. J. Hu, J. W. Locasale, J. H. Bielas, J. O'Sullivan, K. Sheahan, L. C. Cantley, M. G. Vander Heiden, D. Vitkup, Heterogeneity of tumor-induced gene expression changes in the human metabolic network. *Nat. Biotechnol.* **31**, 522–529 (2013).
36. J. R. Cantor, M. Abu-Remaileh, N. Kanarek, E. Freinkman, X. Gao, A. Louissaint Jr., C. A. Lewis, D. M. Sabatini, Physiologic medium rewires cellular metabolism and reveals uric acid as an endogenous inhibitor of UMP synthase. *Cell* **169**, 258–272.e17 (2017).
37. P. Dey, J. Baddour, F. Muller, C. C. Wu, H. Wang, W.-T. Liao, Z. Lan, A. Chen, T. Gutschner, Y. Kang, J. Fleming, N. Satani, D. Zhao, A. Achreja, L. Yang, J. Lee, E. Chang, G. Genovese, A. Viale, H. Ying, G. Draetta, A. Maitra, Y. A. Wang, D. Nagrath, R. A. DePinho, Genomic deletion of malic enzyme 2 confers collateral lethality in pancreatic cancer. *Nature* **542**, 119–123 (2017).
38. F. L. Muller, E. A. Aquilanti, R. A. DePinho, Collateral Lethality: A new therapeutic strategy in oncology. *Trends Cancer* **1**, 161–173 (2015).
39. M. E. Ritchie, B. Phipson, D. Wu, Y. Hu, C. W. Law, W. Shi, G. K. Smyth, limma powers differential expression analyses for RNA-sequencing and microarray studies. *Nucleic Acids Res.* **43**, e47 (2015).
40. S. Le, J. Josse, F. Husson, FactoMineR: An R package for multivariate analysis. *J. Stat. Softw.* **25**, 1–18 (2008).
41. I. Thiele, N. Swainston, R. M. T. Fleming, A. Hoppe, S. Sahoo, M. K. Aurich, H. Haraldsdottir, M. L. Mo, O. Rolfsson, M. D. Stobbe, S. G. Thorleifsson, R. Agren, C. Bölling, S. Bordel, A. K. Chavali, P. Dobson, W. B. Dunn, L. Endler, D. Hala, M. Hucka, D. Hull, D. Jameson, N. Jamshidi, J. J. Jonsson, N. Juty, S. Keating, I. Nookaew, N. L. Novère, N. Malys, A. Mazein, J. A. Papin, N. D. Price, E. S. Sr, M. I. Sigurdsson, E. Simeonidis, N. Sonnenschein, K. Smallbone, A. Sorokin, J. H. G. M. van Beek, D. Weichart, I. Goryanin, J. Nielsen, H. V. Westerhoff, D. B. Kell, P. Mendes, B. Ø. Palsson, A community-driven global reconstruction of human metabolism. *Nat. Biotechnol.* **31**, 419–425 (2013).

Acknowledgments: We thank the members of the Locasale laboratory for comments and support, particularly X. Liu, M. Reid, and M. Liberti for technical assistance. **Funding:** This work was supported by the National Institutes of Health (R01CA193256 to J.W.L., F31CA224973 to S.M.S., and T32GM007184 to V.R.) and by a Graduate Fellowship from the Duke University School of Medicine to S.M.S. **Author contributions:** Conceptualization, S.M.S. and J.W.L.; cell culture experiments, S.M.S.; metabolomics and data analysis, S.M.S. and P.G.M.; mathematical modeling, P.G.M. and Z.D.; all other experiments, S.M.S. and V.R.; and writing, S.M.S. and J.W.L. with essential input from all authors. **Competing interests:** The authors declare that they have no competing interests. **Data and materials availability:** All data needed to evaluate the conclusions in the paper are present in the paper and/or the Supplementary Materials. Additional data related to this paper may be requested from the authors.

Submitted 18 October 2018
Accepted 16 May 2019
Published 26 June 2019
10.1126/sciadv.aav7769

Citation: S. M. Sanderson, P. G. Mikhael, V. Ramesh, Z. Dai, J. W. Locasale, Nutrient availability shapes methionine metabolism in p16/*MTAP*-deleted cells. *Sci. Adv.* **5**, eaav7769 (2019).

Science Advances

Nutrient availability shapes methionine metabolism in p16/*MTAP*-deleted cells

Sydney M. Sanderson, Peter G. Mikhael, Vijyendra Ramesh, Ziwei Dai and Jason W. Locasale

Sci Adv **5** (6), eaav7769.
DOI: 10.1126/sciadv.aav7769